Original Article

Journal of Intelligent Material Systems and Structures

Journal of Intelligent Material Systems and Structures
2015, Vol. 26(5) 489–504

DOI: 10.1177/1045389X14529611
jim.sagepub.com
SAGE

Three-dimensional free vibration of multi-layered piezoelectric plates through approximate and exact analyses

Arcangelo Messina[1] and Erasmo Carrera[2]

Abstract

This article presents two models that have the aim of analysing three-dimensional freely vibrating plates made of an arbitrary combination of structural and/or piezoelectric layers. The first model is derived from a displacement-based variational statement, and it investigates the possibility of approaching exact three-dimensional results at any degree of accuracy. This model has been developed as if the plates were virtually made of a single layer, and it is herein referred to as the approximate analysis model. The second model is based on solving the set of three-dimensional linear equations coupling the relevant mechanical and electric quantities, and it therefore provides exact results. The latter model is derived from the transfer-matrix technique which, having shown numerical instability in the multiphysics problem being dealt with, was then successfully modified to provide exact and reliable results. Excellent agreement has been obtained between the models, and this shows how the exact approach here designed is stably able to overcome ill conditioning problems, while the first model, having been validated by the exact results, could be applied to effectively investigate multiphysics problems for general boundary conditions, and for cross- and/or angle-ply laminates, at any level of required accuracy.

Keywords

Multi-layered plates, piezoelectric plates, exact solutions, theorem of virtual displacements, free vibrating plates, three-dimensional plate analysis

Introduction

Multiphysics processes in which smart materials, based on piezoelectric layers, seem to play an important role in several engineering systems to control vibrations and in health monitoring constitute an important area of research. The piezoelectric layers are generally embedded in structural systems at specific locations; strains may be induced (actuation) on the structure through the application of voltages to the piezoelectric layers, or voltages may be relieved (sensing) during the motion of a structure. In order to successfully incorporate piezoelectric actuators or sensors in structures, the mechanical interaction between such piezoelectric layers and the hosting structure needs to be fully understood. In this context, three-dimensional (3D) models play an important role because of their capacity to accurately describe the relevant physical phenomena. The 3D models are also important due to the fact that they can offer benchmarks that can be used to compare the performance of models as well as to directly investigate phenomena without including approximations.

The first theoretical studies that addressed the analysis of piezoelectric crystal plates can be attributed to Mindlin (1952, 1972). Since then, investigations and models have been taken into account and designed from both a theoretical and a numerical point of view. As far as the specific interests of this article (freely vibrating plates) are concerned, a theoretical treatment of the problem seems to have been lacking in the literature until the beginning of the 1990s, when Yang and Batra (1994) systematically presented an extensive analysis of the eigenvalue problem, associated with the free vibrations of a finite piezoelectric body. In this work (Yang

[1]Dipartimento di Ingegneria dell'Innovazione, Università del Salento, Lecce, Italy
[2]Dipartimento di Ingegneria Meccanica e Aerospaziale, Politecnico di Torino, Torino, Italy

Corresponding author:
Arcangelo Messina, Dipartimento di Ingegneria dell'Innovazione, Università del Salento, s.p. 6, Lecce-Monteroni, 73100 Lecce, Italy.
Email: arcangelo.messina@unisalento.it

and Batra, 1994), the analysis was theoretical, and a series of properties of engineering interest (orthogonality of the modes, reality of the eigenvalues, positivity of the eigenvalues, etc.) were proved theoretically. In almost the same period, Heyliger and Saravanos (1995) presented a 3D exact analysis that enriched the literature with numerical results, regarding both the analyses of single piezoelectric layer and multi-layered plates. The extensive set of numerical values provided by Heyliger and Saravanos (1995) was later used as a benchmark, although numerical difficulties in evaluating the resulting non-linear eigenvalue problem, together with ill-conditioned behaviour, have been pointed out by Cupial (2005). The natural frequencies of a single-layer rectangular piezoelectric plate were calculated in Chen et al. (1998) using a transfer-matrix formulation–based approach. Chen et al. (1998) did not list any numerical results or implement any multi-layered plates. Moreover, Chen et al. (1998) investigated simply supported plates which are suitable for an exact treatment, but not applicable for more general systems. Similarly, Batra and Liang (1997) and Liang and Batra (1997) analysed such a multiphysics problem, related to simply supported boundary conditions, by neglecting dielectric permittivity and assuming that the electric potential was a linear function of the transversal coordinate of the plate. Subsequently, Vel and Batra (2000, 2001) carried out static analyses of 3D deformations of multi-layered piezoelectric rectangular plates using the Eshelby–Stroh formalism. About 5 years later, Ballhause et al. (2005) developed a unified formulation to assess multi-layered theories for piezoelectric plates; equivalent single-layer and layer-wise models were developed to carry out static and dynamic analyses. These analyses regarded simply supported boundary conditions which allowed the authors to obtain solutions within the approximation used in the expansions of the displacement components and electric potential (up to the fourth order through the transversal direction of the plate). It is here stressed that the approximate part of these models only regarded one of the three coordinates (z – out of plane), while the remaining two (x, y – in plane) were fulfilled exactly through circular functions for the particular boundary conditions that were used. Under such assumptions, the higher order model of Ballhause et al. (2005) (i.e. LD4) leads to a quasi-3D description of the dynamic and static responses of the analysed multi-layered plates. These conclusions were reached by comparing their results with those provided by Heyliger and Saravanos (1995). Exact solutions for in-plane polarization cases were provided by Deü and Benjeddou (2005). The basic principles of the models described in Ballhause et al. (2005) were later considered by D'Ottavio and Kröplin (2006) and extended by Carrera et al. (2010) to derive consistent differential electromechanical governing equations through the principle of virtual displacements and Reissner's (1984) mixed variational theorem.

On the basis of the above bibliographical discussion, the need has emerged of an approximate methodology that is able to deal with the 3D dynamics of freely vibrating piezoelectric plates, for general edge boundary conditions, using an expansion level that would allow any degree of accuracy to be considered in a unique formulation for single- or multi-layered piezoelectric plates. Considering multi-layered plates and any classical edge boundary condition is an interesting novelty in the frame of the above-mentioned 3D analyses; however, this becomes additionally interesting, considering the increasing power of modern calculators with which it is possible to naturally extend an approximate analytical technique to well-established numerical techniques (e.g. finite elements). An analytical model is thus introduced through the extended theorem of virtual displacements along with GPSFs (Messina, 2002). GPSFs stand for global piecewise-smooth functions and recall the suitable functional bases that have the aim of modelling multi-layered plates as if they were virtually made up of a single layer; the idea, which was first introduced by Messina (2002), is based on the idea of considering cusps as additional features in an expansion series; in this regard, an algorithmic graph (Messina, 2002) joins piecewise-smooth functions in order to obtain an expansion series that contains discontinuous derivatives; this expansion is able to model non-smooth functions (displacement components and electric quantities) without suffering from the so-called Gibbs phenomenon. For the sake of brevity, the GPSFs are not shown here; the readers can refer to the works of Messina (2002, 2005, 2011) and Messina and Rollo (2010) for further details.

Moreover, since this article has the aim of demonstrating the capacity of the approximate analytical model to attain exact 3D-results, the latter have been derived through an exact analysis for simply supported boundary conditions. This second model, which is based on the transfer-matrix technique (e.g. Fan and Ye, 1990; Messina, 2012), can be considered valuable. The original transfer-matrix technique, which is related to the use of an exponential matrix (e.g. Boyce and DiPrima, 1997), in fact appears to be remarkably unstable for the multiphysics problem being dealt with, and for this reason, a modified technique was needed to provide exact and reliable results.

Although the approaches of the presented models are substantially different, excellent agreement has been obtained, thus showing how the exact analysis is stable and able to overcome ill conditioning problems, while the approximated approach can be extended naturally to numerical schemes in order to conduct advanced 3D analysis. Finally, comparisons with previous results have also been made, thus showing that the present results could be useful benchmarks for future comparisons.

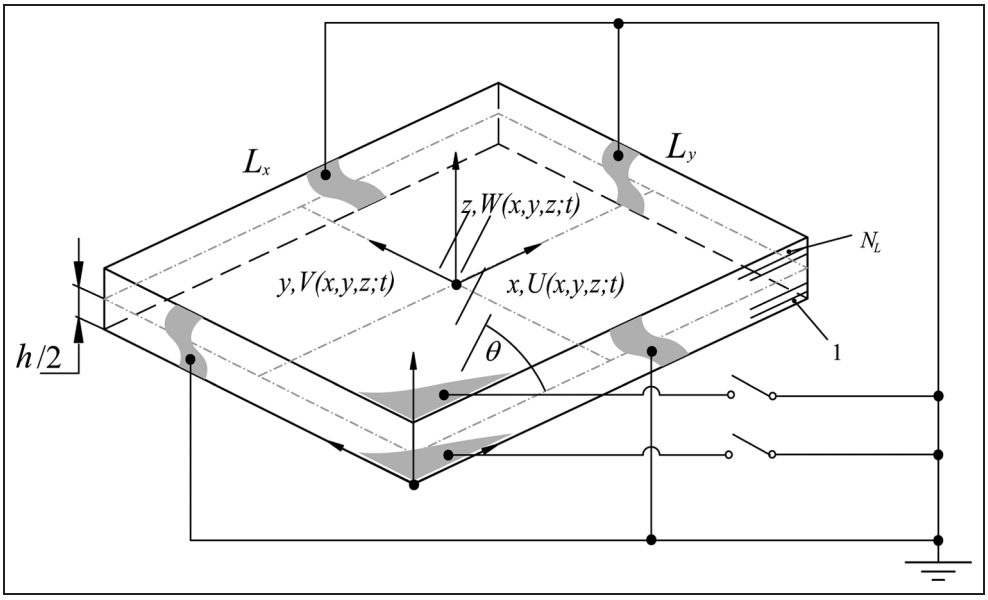

Figure 1. Nomenclature of an N_L layer elastic piezoelectric plate.

Theoretical description of the boundary value problem

Basic assumptions

The problem this article is dealing with is based on Figure 1 where an anisotropic linear elastic plate of arbitrary span to thickness ratio made of N_L composite/piezoelectric layers (thickness and density h_k and ρ_k, respectively, with $k = 1, ..., N_L$)) is subjected to arbitrary although classical boundary conditions. The system of coordinates has the origin placed at the geometric centre of the plate when the approximate analysis is taken into account, while it is alternatively moved at the bottom-corner of the plate when the exact approach is described; these different choices are due to the analytical simplicity gained from both the models.

The boundary conditions, depicted in Figure 1, concern mechanical (displacement or stresses) and electric (potential or charges) entities both on the lateral edges and bottom/top of the plate. In particular, with regard to Figure 1, CSSFCF would refer to boundary conditions for mechanical entities: Clamped ($x = -L_x/2$), Supported ($x = L_x/2$), Supported ($y = -L_y/2$), Free ($y = L_y/2$), Clamped ($z = -h/2$) and Free ($z = h/2$). The same order on the respective surfaces would mean Grounded (nil potential) through the letter G, while the letter F would relate to nil charge (Free Potential).

The present formulation is based on quasi-static assumption of the electric field along with the small displacement assumptions. The extended theorem of virtual displacements (1) is able to derive the relevant governing equations along with the consistent boundary conditions

$$\int_{Vol} \left[\boldsymbol{\sigma}^{\mathrm{T}}\delta\boldsymbol{\varepsilon} + \delta_d\rho\left(\ddot{U}\delta U + \ddot{V}\delta V + \ddot{W}\delta W\right) - \mathbf{D}^{\mathrm{T}}\delta\mathbf{E}\right]\mathrm{d}Vol = \int_{Sur} \left[\delta_s(\bar{X}_n\delta U + \bar{Y}_n\delta V + \bar{Z}_n\delta W) - \bar{q}\delta\varphi\right]\mathrm{d}Sur \tag{1}$$

The terms ($\bar{X}_n$, $\bar{Y}_n$, $\bar{Z}_n$) and $\bar{q}$ are surface loads and free electric charge, respectively, prescribed on the boundary surface of the body (Sur); φ is the electric potential; $\mathbf{D}^{\mathrm{T}}$ is the electric displacement field (D_x, D_y, D_z); $\mathbf{E}^{\mathrm{T}}$ corresponds to the electric field (E_x, E_y, E_z); ρ is the material density; (U, V, W) are the displacement components associated with the generic point of the body; $\boldsymbol{\sigma}^{\mathrm{T}}$ represents the symmetric stress tensor (σ_x, σ_y, σ_z, τ_{yz}, τ_{xz}, τ_{xy}); while, finally, $\boldsymbol{\varepsilon}^{\mathrm{T}}$ represents the symmetric strain tensor (ε_x, ε_y, ε_z, γ_{yz}, γ_{xz}, γ_{xy}). Both the symbols (δ_s, δ_d) would be tracers for giving the possibility to develop static and/or dynamic models; in the present context, only dynamic analysis is taken into account (i.e. $\delta_s = 0$, $\delta_d = 1$).

The variational statement in equation (1) along with (*i*) suitable integrations by part, (*ii*) equations (2) and (3)

$$\varepsilon_x = \frac{\partial U}{\partial x} = U_{,x}, \quad \varepsilon_y = \frac{\partial V}{\partial y} = V_{,y}, \quad \varepsilon_z = \frac{\partial W}{\partial z} = W_{,z}$$
$$\gamma_{xy} = U_{,y} + V_{,x}, \quad \gamma_{yz} = W_{,y} + V_{,z}, \quad \gamma_{xz} = W_{,x} + U_{,z} \tag{2}$$

$$E_x = -\frac{\partial\varphi}{\partial x} = -\varphi_{,x}, \quad E_y = -\frac{\partial\varphi}{\partial y} = -\varphi_{,y}, \quad E_z = -\frac{\partial\varphi}{\partial z} = -\varphi_{,z} \tag{3}$$

and (*iii*) prescribed essential boundary conditions (on displacement components and electric potential) is able to provide the following differential equations

$$\begin{aligned}\sigma_{x,x}+\tau_{xy,y}+\tau_{xz,z}&=\rho\ddot{U}\\ \tau_{yx,x}+\sigma_{y,y}+\tau_{yz,z}&=\rho\ddot{V}\\ \tau_{zx,x}+\tau_{zy,y}+\sigma_{z,z}&=\rho\ddot{W}\\ D_{x,x}+D_{y,y}+D_{z,z}&=0\end{aligned}\tag{4}$$

and the consistent natural boundary conditions

$$\begin{aligned}&\bar{X}_n,\ \bar{Y}_n,\ \bar{Z}_n \quad \text{at } Sur\\ &\mathbf{D}\circ\mathbf{n}=-\bar{q} \quad \text{at } Sur\end{aligned}\tag{5}$$

where $\mathbf{n}$ is the normal versor at boundary surface (Sur) and ($\circ$) means dot product ($\mathbf{D}\circ\mathbf{n}=D_n$).

In order to complete the full set of equations governing the electromechanical behaviour of the plate, the following constitutive equations are taken into account

$$\begin{aligned}\boldsymbol{\sigma}&=\mathbf{C}\cdot\varepsilon-\mathbf{e}^{\mathrm{T}}\mathbf{E}\\ \mathbf{D}&=\mathbf{e}\cdot\varepsilon+\in\cdot\mathbf{E}\end{aligned}\tag{6}$$

In equation (6), $\mathbf{C}$, $\mathbf{e}$ and $\in$ (elastic stiffness, piezoelectric and permittivity matrices, respectively) couple the mechanical entities with those electric and correspond to the following explicit expressions

$$\mathbf{C}=\begin{bmatrix}C_{11}&C_{12}&C_{13}&0&0&C_{16}\\ &C_{22}&C_{23}&0&0&C_{26}\\ &&C_{33}&0&0&C_{36}\\ &&&C_{44}&C_{45}&0\\ &sym&&&C_{55}&0\\ &&&&&C_{66}\end{bmatrix};$$

$$\mathbf{e}=\begin{bmatrix}0&0&0&e_{14}&e_{15}&0\\ 0&0&0&e_{24}&e_{25}&0\\ e_{31}&e_{32}&e_{33}&0&0&e_{36}\end{bmatrix}\in=\begin{bmatrix}\in_1&0&0\\ 0&\in_2&0\\ 0&0&\in_3\end{bmatrix}\tag{7}$$

The approximate analysis

The present model starts by inserting a suitable expansion of both the displacement and the electric potential fields (8) into the variational statement (1) and by applying the virtual operator by keeping ($X(x)$, $Y(y)$, $Z(z)$) as known functional bases while A coefficients are unknowns

$$\begin{cases}U(x,y,z;t)=e^{i\omega t}\sum_{l}^{L_u}\sum_{m}^{M_u}\sum_{n}^{N_u}A^u_{lmn}X^u_l(x)\cdot Y^u_m(y)\cdot Z^u_n(z)=e^{i\omega t}(\mathbf{X}^u\mathbf{Y}^u\mathbf{Z}^u)^{\mathrm{T}}(\mathbf{A}^u)\\ V(x,y,z;t)=e^{i\omega t}\sum_{l}^{L_v}\sum_{m}^{M_v}\sum_{n}^{N_v}A^v_{lmn}X^v_l(x)\cdot Y^v_m(y)\cdot Z^v_n(z)=e^{i\omega t}(\mathbf{X}^v\mathbf{Y}^v\mathbf{Z}^v)^{\mathrm{T}}(\mathbf{A}^v)\\ W(x,y,z;t)=e^{i\omega t}\sum_{l}^{L_w}\sum_{m}^{M_w}\sum_{n}^{N_w}A^w_{lmn}X^w_l(x)\cdot Y^w_m(y)\cdot Z^w_n(z)=e^{i\omega t}(\mathbf{X}^w\mathbf{Y}^w\mathbf{Z}^w)^{\mathrm{T}}(\mathbf{A}^w)\\ \varphi(x,y,z;t)=e^{i\omega t}\sum_{l}^{L\varphi}\sum_{m}^{M_\varphi}\sum_{n}^{N_\varphi}A^\varphi_{lmn}X^\varphi_l(x)\cdot Y^\varphi_m(y)\cdot Z^\varphi_n(z)=e^{i\omega t}(\mathbf{X}^\varphi\mathbf{Y}^\varphi\mathbf{Z}^\varphi)^{\mathrm{T}}(\mathbf{A}^\varphi)\end{cases}\tag{8}$$

Equations (8) illustrate two alternative expressions in order to simplify the related algebraic differential manipulations. In this regard, the notation of the third member is taken into account where the couple ($\mathbf{X}^{u,v,w,\phi}$, $\mathbf{Y}^{u,v,w,\phi}$, $\mathbf{Z}^{u,v,w,\phi}$) and ($\mathbf{A}^{u,v,w,\phi}$) represent two vectors whose arrangement, for example, for U and $L_u=M_u=N_u=2$, is shown in equation (9)

$$\begin{aligned}(\mathbf{X}^u\mathbf{Y}^u\mathbf{Z}^u)^{\mathrm{T}}&=(X^u_1Y^u_1Z^u_1,X^u_1Y^u_1Z^u_2,X^u_1Y^u_2Z^u_1,X^u_1Y^u_2Z^u_2,X^u_2Y^u_1Z^u_1,X^u_2Y^u_1Z^u_2,X^u_2Y^u_2Z^u_1,X^u_2Y^u_2Z^u_2)\\ (\mathbf{A}^u)^{\mathrm{T}}&=(A^u_{111},A^u_{112},A^u_{121},A^u_{122},A^u_{211},A^u_{212},A^u_{221},A^u_{222})\end{aligned}\tag{9}$$

The formulation will result in an infinite system of equations in infinite unknowns when $L, M, N\to\infty$. Of course, the truncation of the relevant expansions will provide the related approximate solutions. Therefore, such an analytical process combined with equations (2), (3) and (6) provides the eigenvalue problem fully described in the appendix.

At this stage of development, it should be evident that the model is unaware of whether the particular functional bases can be globally assumed in the relevant domains (i.e. $x, y\in[-L_{x,y}/2, L_{x,y}/2]$, $z\in[-h/2, h/2]$). The functional bases ($X(x)$, $Y(y)$, $Z(z)$) should fulfil the essential boundary conditions at external boundary surface (Sur) and at interlaminar levels in the presence or absence of multiple layers. In particular, the functional bases (X, Y) should fulfil the essential boundary conditions at $(x, y)=-L_{x,y}/2, L_{x,y}/2$ and are assumed to be classical polynomials (smooth functions); in this case, any inner condition is not present due to the absence of in-plane material/geometric discontinuities. Instead, the functional z-bases should fulfil the essential boundary conditions at $(z)=-h/2, h/2$ and are assumed smooth, such as classical polynomials, only when single-layer plates are taken into account; when multilayers are stacked, such z-functional bases must correspond to GPSFs (Messina, 2002; Messina and Rollo, 2010) in order to potentially allow continuous or discontinuous stresses.

Based on a non-dimensional domain $[-1/2, 1/2]$, the geometric condition regarding the so-called s-end (supported) is characterized by each functional component constrained to satisfy the following condition

$$f(-1/2 \text{ or } 1/2)_i=0;\quad \text{for any } i\tag{10}$$

while in the case of the so-called f-end (or free), each single component of the functional base is not constrained at all

$$f(-1/2)_i, f(1/2)_i \quad \text{no constraint for any } i \qquad (11)$$

It is stressed here that conditions (10) and (11) are identified as s-end (supported) and f-end (free), respectively, although they could not have a respective physical meaning. The adopted lowercase letters (s, f) indicate geometric conditions of the functional components (equations (10) and (11)) rather than physical boundary conditions (C, S, F). When the lateral surface at $x = -L_x/2$ is physically clamped (i.e. U, V and W nil at $x = -L_x/2$), X_l^u, X_l^v and X_l^w for any l in equation (8) are s-end components (equation (10)). Conversely, a 3D simply supported end involves both conditions (10) and (11), while a completely free end needs conditions (11) alone.

There exist several ways to build suitable admissible bases once the essential edge boundary conditions (10) and (11) are established for each displacement component; here, a base is assumed orthonormal in its own local domain and is obtained by using a recursive procedure (e.g. Messina and Rollo, 2010). Equations (12) provide explicit expressions in the non-dimensional domain $\xi \in [-1/2, 1/2]$ for three essential-type boundary conditions.

kth member	ss-base	ff-base	sf-base
$f_1(\xi)$	$\xi^2 - 1/4$	1	$\xi + 1/2$
$f_2(\xi)$	$\xi^3 - \xi/4$	ξ	$\xi^2 + \xi/4 - 1/8$

$$f_k(\xi) \text{ for } k>2 \quad B_k = \int_{[-1/2,1/2]} \xi f_{k-1}^2(\xi)\mathrm{d}\xi \Big/ \int_{[-1/2,1/2]} f_{k-1}^2(\xi)\mathrm{d}\xi$$
$$C_k = \int_{[-1/2,1/2]} \xi f_{k-1}(\xi) f_{k-2}(x)\mathrm{d}\xi \Big/ \int_{[-1/2,1/2]} f_{k-2}^2(\xi)\mathrm{d}\xi$$
$$(\xi - B_k) f_{k-1}(\xi) - C_k f_{k-2}(\xi) \qquad (12)$$

The members in equation (12) should be divided by the square root of their own norms in order to provide normal bases. Due to the fact that this study is 3D, the bases in equation (12) cover any combination of classical boundary conditions (C, F, S). In order to better clarify what has just been mentioned, regarding boundary conditions mentioned above for Figure 1 with $N_L = 3$, equation (13) illustrates the bases that should be used into the model for CSSFFF-GGGGFF

In equations (13), the z-domain has been partitioned into three sub-domains (having assumed $N_L = 3$), and here, GPSFs are required; the choice for the electric potential at bottom and top layers (ff or sf and ff or fs) depends on the state of the switches in Figure 1 if they are both off (open circuit) or on (closed circuit or short circuit), respectively. Let us finally notice that a nil potential is modelled through an s-end (equation (10)), while a nil charge (free potential) is modelled through an f-end (equation (11)).

It is finally stressed that when the expansion (8) is truncated up to N terms (by letting $L = M = N$) in endorsement to equation (35), the first N polynomial terms are simply being used; however, this is not the case when the GPSFs are taken into account. Indeed, in this latter case, if N_L is referred to the number of transversal sub-domains and N_o the number of polynomial terms in bases (12) and (13), the number of GPSFs corresponds to $N = N_L(N_o - 1) + 1$, and therefore, the expansion for the z-terms (N) is different with respect to x, y terms ($L = M = N_o$).

Appendix 1, and specifically equation (34), makes it clear that the eigenvalues can be extracted by recurring to specific routines applied on the classical generalized first-order eigenvalue and eigenvector problem: $(\mathbf{K} - \omega^2\mathbf{M})\mathbf{A} = 0$.

The exact analysis

The present 3D model is based on the resolution of 3D equilibrium equation (4) with regard to a multi-layer plate made of structural/piezoelectric laminates. For this model, the plate is made of cross-ply laminates ($C_{16} = C_{26} = C_{36} = C_{45} = 0$) and is subjected to mechanical simply supported lateral boundary conditions along with top and bottom surfaces completely free. Such boundary conditions are needed in order to implement an exact analysis and validate the model described in the previous section; this latter model, conversely, can be applied for any classical boundary conditions and for both cross- and/or angle-ply laminates placed in an arbitrary stacking sequence. Moreover, from an electric point of view, the layers have $e_{14} = e_{25} = e_{36} = 0$, the lateral boundary surface is grounded ($\varphi = 0$), while the top and bottom surfaces can be both grounded ($\varphi = 0$) and free ($q = 0$).

The following conditions explicate both essential and natural boundary conditions with regard to the

$$\begin{array}{l}
X(x)_1^u, X(x)_2^u, \ldots \text{ sf base; } Y(y)_1^u, Y(y)_2^u, \ldots \text{ sf base; } Z(z)_1^u, Z(z)_2^u, \ldots \text{ ff base, ff base, ff base} \\
X(x)_1^v, X(x)_2^v, \ldots \text{ ss base; } Y(y)_1^v, Y(y)_2^v, \ldots \text{ ff base; } Z(z)_1^v, Z(z)_2^v, \ldots \text{ ff base, ff base, ff base} \\
X(x)_1^w, X(x)_2^w, \ldots \text{ ss base; } Y(y)_1^w, Y(y)_2^w, \ldots \text{ sf base; } Z(z)_1^w, Z(z)_2^w, \ldots \text{ ff base, ff base, ff base} \\
X(x)_1^\varphi, X(x)_2^\varphi, \ldots \text{ ss base; } Y(y)_1^\varphi, Y(y)_2^\varphi, \ldots \text{ ss base; } Z(z)_1^\varphi, Z(z)_2^\varphi, \ldots \text{ sf base, ff base, ff base}
\end{array} \qquad (13)$$

system of coordinate placed at the bottom-corner of the plate (Figure 1)

$$\begin{cases} \tau_{xz} = \tau_{yz} = \sigma_z = 0, \quad (\varphi = 0 \; or \; q = 0) & z = 0, \; h \\ W = V = 0, \; \sigma_x = 0, \; \varphi = 0 & x = 0, \; L_x \\ W = U = 0, \; \sigma_y = 0, \; \varphi = 0 & y = 0, \; L_y \end{cases} \tag{14}$$

while equations (15) show both essential and natural boundary conditions at each kth interface (located at $z_k = \sum_j^k h_j$ with $k = 1, ..., N_L - 1$) between two consecutive layers. In this latter regard, apexes in parentheses shown in equations (15) refer to the relevant quantities of the kth layer

$$\begin{cases} \sigma_z^{(k+1)}(z_k) = \sigma_z^{(k)}(z_k); & U^{(k+1)}(z_k) = U^{(k)}(z_k) \\ \tau_{yz}^{(k+1)}(z_k) = \tau_{yz}^{(k)}(z_k); & V^{(k+1)}(z_k) = V^{(k)}(z_k) \\ \tau_{xz}^{(k+1)}(z_k) = \tau_{xz}^{(k)}(z_k); & W^{(k+1)}(z_k) = W^{(k)}(z_k) \\ \varphi^{(k+1)}(z_k) = \varphi^{(k)}(z_k); & D_z^{(k+1)}(z_k) = D_z^{(k)}(z_k) \end{cases}$$
$$\text{for } k = 1, \ldots, N_L - 1 \tag{15}$$

Therefore, based on the above-mentioned assumptions, the 3D model is first developed by transforming the system of partial differential equations into the system of ordinary differential equations (ODEs). Such a transformation is essentially accomplished by assuming the following displacement field

$$\begin{cases} U(x,y,z;t) = u(z) \cdot \cos(q_x \cdot x) \cdot \sin(q_y \cdot y) \cdot \cos(\omega \cdot t) \\ V(x,y,z;t) = v(z) \cdot \sin(q_x \cdot x) \cdot \cos(q_y \cdot y) \cdot \cos(\omega \cdot t) \\ W(x,y,z;t) = w(z) \cdot \sin(q_x \cdot x) \cdot \sin(q_y \cdot y) \cdot \cos(\omega \cdot t) \\ \varphi(x,y,z;t) = \phi(z) \cdot \sin(q_x \cdot x) \cdot \sin(q_y \cdot y) \cdot \cos(\omega \cdot t) \end{cases} \tag{16}$$

which fulfils the lateral boundary conditions (i.e. at $x = 0, L_x$ and $y = 0, L_y$ in equation (14)) of the plate; in equation (16), $q_x = m\pi/L_x$ and $q_y = n\pi/L_y$, (m, n) are the number of half waves in the in-plane domain, and finally, $(u(z), v(z), w(z), \phi(z))$ are unknown functions to be determined. The ODEs system can be obtained by substituting equations (16) into equation (4) once these latter have been previously written in function of displacements and electric potential through equations (2), (3) and (6). Therefore, simplifying the synchronous temporal part, the following system of ODEs can be achieved

$$\hat{\mathbf{A}} \cdot \begin{pmatrix} u \\ v \\ w \\ \phi \end{pmatrix} + \hat{\mathbf{B}} \cdot \begin{pmatrix} u' \\ v' \\ w' \\ \phi' \end{pmatrix} + \widehat{\mathbf{C}} \cdot \begin{pmatrix} u'' \\ v'' \\ w'' \\ \phi'' \end{pmatrix} = \begin{pmatrix} 0 \\ 0 \\ 0 \\ 0 \end{pmatrix} \tag{17}$$

being the apexes $()'$ representative of the ordinary differential operator $\mathrm{d}()/\mathrm{d}z$, while matrices $(\hat{\mathbf{A}}, \hat{\mathbf{B}}, \widehat{\mathbf{C}})$ have the following explicit expressions

$$\hat{\mathbf{A}} = \begin{bmatrix} \omega^2 - (C_{11}q_x^2 + C_{66}q_y^2) & -q_xq_y(C_{12} + C_{66}) & 0 & 0 \\ -q_xq_y(C_{12} + C_{66}) & \omega^2 - (C_{22}q_y^2 + C_{66}q_x^2) & 0 & 0 \\ 0 & 0 & \omega^2 - (C_{44}q_y^2 + C_{55}q_x^2) & -(e_{15}q_x^2 + e_{24}q_y^2)W_\varphi \\ 0 & 0 & -(e_{15}q_x^2 + e_{24}q_y^2) & (\in_1 q_x^2 + \in_2 q_y^2)W_\varphi \end{bmatrix} \tag{18}$$

$$\hat{\mathbf{B}} = \begin{bmatrix} 0 & 0 & (C_{13} + C_{55})q_x & (e_{15} + e_{31})q_xW_\phi \\ 0 & 0 & (C_{23} + C_{44})q_y & (e_{24} + e_{32})q_yW_\phi \\ -(C_{13} + C_{55})q_x & -(C_{23} + C_{44})q_y & 0 & 0 \\ -(e_{15} + e_{31})q_x & -(e_{24} + e_{32})q_y & 0 & 0 \end{bmatrix} \tag{19}$$

$$\widehat{\mathbf{C}} = \begin{bmatrix} C_{55} & 0 & 0 & 0 \\ 0 & C_{44} & 0 & 0 \\ 0 & 0 & C_{33} & e_{33}W_\varphi \\ 0 & 0 & e_{33} & -\in_{33} W_\varphi \end{bmatrix} \tag{20}$$

In particular $\widehat{\mathbf{C}}$ can be symbolically inverted to get $\hat{\mathbf{C}}$ (equation (21)) and write ODEs system (17) in its canonical form (22)

$$\hat{\mathbf{C}} = \widehat{\mathbf{C}}^{-1} = \frac{-1}{(e_{33}^2 + C_{33} \cdot \in_3)} \begin{bmatrix} (e_{33}^2 + C_{33} \cdot \in_3)/C_{55} & 0 & 0 & 0 \\ 0 & (e_{33}^2 + C_{33} \cdot \in_3)/C_{44} & 0 & 0 \\ 0 & 0 & \in_3 & e_{33} \\ 0 & 0 & e_{33}/W_\varphi & -C_{33}/W_\varphi \end{bmatrix} \tag{21}$$

$$\mathbf{F}(z)' = \begin{pmatrix} u' \\ v' \\ w' \\ \phi' \\ u'' \\ v'' \\ w'' \\ \phi'' \end{pmatrix} = \underbrace{\begin{bmatrix} \mathbf{0}_{4\times4} & \mathbf{I}_{4\times4} \\ \hat{\mathbf{C}}\cdot\hat{\mathbf{A}} & \hat{\mathbf{C}}\cdot\hat{\mathbf{B}} \end{bmatrix}}_{\mathbf{G}} \begin{pmatrix} u \\ v \\ w \\ \phi \\ u' \\ v' \\ w' \\ \phi' \end{pmatrix} = \mathbf{G}\cdot\mathbf{F}(z) \tag{22}$$

where, for better intelligibility, terms in $\mathbf{F}(z)$ have been shown in equation (22) with their physical meaning rather than in their canonical form (e.g. Boyce and DiPrima, 1997) as first derivative terms (i.e. $y'_1, y'_2, y'_3, y'_4, y'_5, y'_6, y'_7, y'_8$) and related functions (i.e. y_1, y_2, y_3, y_4, y_5, y_6, y_7, y_8) at first and second members, respectively.

The scalar term W_φ, in equations (18) to (21) should be theoretically set equal to 1; however, numerical reasons suggested to substitute in equation (17) a scaled potential function ($\bar{\phi}(z)$) through equation (23)

$$\phi(z) = W_\varphi \cdot \bar{\phi}(z) \tag{23}$$

Such a substitution in equation (17) does not clearly affect the ODE system; indeed, a fictitious scaled unknown function ($\bar{\phi}(z)$) has to be determined in place of the original one ($\phi(z)$) while the latter can be recovered through equation (23). On the other hand, such a substitution of equation (23) into equation (17) is clearly admissible because we are substituting an unknown ($\phi(z)$) with another unknown ($\bar{\phi}(z)$). At the same time, the coefficient (*a priori* set) W_φ is consequently allocated in the matrices ($\hat{\mathbf{A}}$, $\hat{\mathbf{B}}$, $\hat{\mathbf{C}}$). Same treatment has been hereafter developed for the subsequent boundary and interlaminar conditions. For this reason, the analytical formulation is established through a fictitious scaled unknown function $\bar{\phi}(z)$ in place of the original z-potential function $\phi(z)$.

When the plate is made by a single layer, the boundary conditions at the bottom and top of the plate (i.e. at $z = 0, h$ in equation (14)) are the only remaining conditions needed to complete the model as associated with the whole set of 3D equations. These boundary conditions at the top and bottom, in case of nil potential at $z = 0, h$, can be expressed as in equation (24)

$$\tilde{\mathbf{A}}\cdot\mathbf{F}(0,h) = \begin{bmatrix} -q_x C_{13} & -q_y C_{23} & 0 & 0 & 0 & 0 & C_{33} & W_\varphi e_{33} \\ 0 & 0 & q_y C_{44} & W_\varphi q_y e_{24} & 0 & C_{44} & 0 & 0 \\ 0 & 0 & q_x C_{55} & W_\varphi q_x e_{15} & C_{55} & 0 & 0 & 0 \\ 0 & 0 & 0 & W_\varphi & 0 & 0 & 0 & 0 \end{bmatrix} \cdot \mathbf{F}(0,h) = \mathbf{0} \tag{24}$$

when nil electric charge has to be imposed at $z = 0, h$, the last row in $\tilde{\mathbf{A}}$ must be substituted by ($-q_x{\cdot}e_{31}$, $-q_y{\cdot}e_{31}$, 0, 0, 0, 0, e_{33}, $-\in_3{\cdot}W_\varphi$).

Therefore, based on the fact that the solution of equation (22) can be expressed as follows (Boyce and DiPrima, 1997)

$$\mathbf{F}(z) = \exp(\mathbf{G}\cdot z)\cdot\mathbf{F}(0) = \mathbf{P}(z)\cdot\mathbf{F}(0) \tag{25}$$

the exact eigenvalue problem is finally obtained by imposing the boundary conditions (24) along with expression (25)

$$\begin{bmatrix} \tilde{\mathbf{A}}\cdot\mathbf{P}(h) \\ \tilde{\mathbf{A}} \end{bmatrix} \cdot \mathbf{F}(0) = \mathbf{D}(m, n, \omega)\cdot\mathbf{F}(0) = \mathbf{0} \tag{26}$$

In particular, the eigenvalues (ω) can be obtained by equation (26) by looking for ω which nullifies the determinant of $\mathbf{D}$ ($|\mathbf{D}|$). Therefore, the model herein described requires the evaluation of the exponential matrix exp($\mathbf{G}$·h) and the subsequent evaluation of a determinant in ω domain (with (m, n) established in advance). Once the eigenvalues are identified, equations (26) and (25) allow the evaluation of $\mathbf{F}(0)$ and $\mathbf{F}(z)$, respectively, and iteratively.

When the plate is made up of multiple layers, formulations (24) to (26) need to include the interlaminar conditions (15). This can be accomplished by recurring to the concept of transfer matrix (e.g. Fan and Ye, 1990; Messina, 2012) in order to preserve the order of the problem (8 × 8) and thus achieving a formulation which is independent of the number of layers. In particular, by fixing the attention on the kth interface ($k = 1, \ldots, N_L - 1$), the following condition can be written

$$\mathbf{F}^{(k)}(z_k) = \exp(\mathbf{G}^{(k)}\cdot(z_k - z_{k-1})) = \mathbf{P}^{(k)}(z_k - z_{k-1})\cdot\mathbf{F}^{(k)}(z_{k-1}) \tag{27}$$

being the apexes representative of the kth layer. Based on the same nomenclature of equation (27), the continuity conditions (15) can be written as in equation (28), where $\mathbf{T}$ is a matrix

$$\mathbf{F}^{(k+1)}(z_k) = \mathbf{T}(z_k)\cdot\mathbf{F}^{(k)}(z_k) \tag{28}$$

representative of the continuity conditions (15) as proved and explicitly shown in closed form in Appendix 2.

Therefore, recursively imposing the continuity condition (28) along with solutions (27) from the bottom to the top of the multi-layered plate, the following equation is achieved

$$\mathbf{F}^{(N_L)}(h) = \underbrace{\mathbf{P}^{(N_L)}\cdot\mathbf{T}(z_{N_L-1})\cdot\mathbf{P}^{(N_L-1)}\cdot\ldots\cdot\mathbf{P}^{(1)}}_{\mathbf{H}}\cdot \mathbf{F}^{(1)}(0) = \mathbf{H}\cdot\mathbf{F}^{(1)}(0) \tag{29}$$

Based on equation (29), formulation (26) can be regained as in equation (30); slight variations are due to the fact that the bottom and top boundary conditions regard two different layers, and therefore, two different matrices $\tilde{\mathbf{A}}^{(1,N_L)}$ must be taken into account

$$\begin{bmatrix} \tilde{\mathbf{A}}^{(N_L)} \cdot \mathbf{H} \\ \tilde{\mathbf{A}}^{(1)} \end{bmatrix} \cdot \mathbf{F}^{(1)}(0) = (\mathbf{0}) \tag{30}$$

Equation (30), similarly to equation (26), can be used to extract eigenvalues and relevant eigenvectors in case of multi-layered plates.

At this stage, before closing this section, a discussion related to the numerical needs of the present model is required. The present model is substantially different from the model presented in section 'The approximate analysis'. Indeed, such a model allows to extract the exact eigenvalues by displaying the autofunction *determinant* ($\mathbf{D}(\omega, m, n)$) and by looking for its roots (the eigenvalues); conversely, the approximate analysis is based on the extraction of the eigenvalues by numerically solving a classical generalized first-order eigenvalue and eigenvector problem (31).

The model shown in this section is essentially based on equation (30) (or equation (26) for single-layer plate) and basically needs the numerical evaluation of (*i*) exponential matrices (dimensions 8×8), (*ii*) determinants, and finally (*iii*) a suitable numerical roots finder extracting the relevant eigenvalues. Such evaluations must be carried out in ω domain with appreciable resolution in order to identify the bounds for each zero (eigenvalue). As far as the first two numerical tools (*i, ii*) are concerned, the built-in functions in MATLAB (R2013a, 64-bit machine) have been used (*det*(), *expm*(), respectively) in all calculations. For the numerical roots finder, the bisection method was implemented. Once the described model was implemented along with the mentioned tools and settling $W_\varphi = 1$, serious numerical instabilities made the model unable to display the autofunction $\det(\mathbf{D}(\omega, m, n))$ for evaluating the eigenvalues. A perusal of the involved equations, along with the sensitivity of the exponential matrix, suggested the way of overcoming such numerical instabilities; the substitution of the true unknown z-potential function ($\phi(z)$) with a fictitious unknown function ($\bar{\phi}(z)$) has resulted to be successful. This substitution is evidently due to the different nature of the involved quantities and equations (i.e. displacement and electric potential fields) which could not be numerically balanced as the model exhibits numerical instabilities.

In spite of the simplicity of position (23), the present model has shown numerical stability insomuch as highly accurate eigenvalues have been evaluated, as shown in the following section.

Table 1. Elastic and electric material properties of single- and multi-layered plates.

Properties	m_1	m_2	m_3
E_1 (GPa)	237.0	81.3	132.38
E_2 (GPa)	23.2	81.3	10.756
E_3 (GPa)	10.5	64.5	10.756
G_{23} (GPa)	2.15	25.6	3.606
G_{13} (GPa)	4.4	25.6	5.6537
G_{12} (GPa)	6.43	30.6	5.6537
ν_{23}	0.177	0.432	0.49
ν_{13}	0.178	0.432	0.24
ν_{12}	0.154	0.329	0.24
e_{14} (C/m^2)	0.0	0.0	0.0
e_{15} (C/m^2)	−0.01	12.72	0.0
e_{24} (C/m^2)	−0.01	12.72	0.0
e_{25} (C/m^2)	0.0	0.0	0.0
e_{31} (C/m^2)	−0.13	−5.2	0.0
e_{32} (C/m^2)	−0.14	−5.2	0.0
e_{33} (C/m^2)	−0.28	15.08	0.0
e_{36} (C/m^2)	0.0	0.0	0.0
$\in_1$ (nF/m)	0.1107	13.06	0.0309897
$\in_2$ (nF/m)	0.1061	13.06	0.026563
$\in_3$ (nF/m)	0.1061	11.51	0.026563
ρ (kg/m^3)	1.0	1.0	1.0

Numerical comparisons and discussion

All the subsequent evaluations and comparisons have been carried out for plates with the material and geometrical properties adopted in Heyliger and Saravanos (1995) and Carrera et al. (2010) and which are here re-listed in Tables 1 and 2. The simulations regard a homogeneous single-layer plate (Pa-plate ref. in Table 2) and four different multi-layered plates (Pb–Pd plate ref., in Table 2).

Tables 3 to 6 illustrate the performance of both of the models presented in section 'Theoretical description of the boundary value problem', with reference to the homogeneous plate (Pa), while the remaining Tables 7 to 10 illustrate the performance of both models with respect to multi-layered plates (Pb–Pd).

Tables 3 and 4 take into account two different electrical boundary conditions at the bottom and top of the plate, respectively, namely, nil electric potential and charge. The exact and approximate results are shown in these tables. The approximate analysis has been carried out both with classical orthogonal polynomials (last three columns), expanded intra the single layer through the z-coordinate, and GPSFs (columns 6–8) developed in two fictitious layers through the whole thickness of the plate. The exact results have been obtained using three different weights, starting from $W_\varphi = 10^6$; in this specific context, it could be of interest to point out that the relevant model showed serious numerical instabilities when values lower than 10^6 (i.e. $W_\varphi = 1, 1000$) were considered.

The model was instead found free from any numerical instability when $W_\varphi \geq 10^6$, and the model could thus be used to stably identify the results shown in Tables 3 and 4; such exact results are in excellent agreement with the approximate results (on six significant digits, regardless of the used base: classical polynomials or GPSFs). The excellent agreement between these two models can be considered remarkable for various reasons. First, the mentioned excellent agreement, on six significant digits, is obtained using two models that are essentially based on different methods; second, the approximate analysis stably approaches the exact results, regardless of which base is used and (in the case of used GPSFs) even without explicitly introducing the relevant continuity conditions at interlaminar levels, thus leaving the responsibility to the GPSFs and the variational statement (1) to converge to exact results; finally, the approximate analysis is based on a classical variational statement that does not require specific numerical treatments, and this makes it suitable for use for numerical designs and/or to analytically investigate different boundary conditions in multiphysics problems. This behaviour of the approximate analysis, used in conjunction with GPSFs, has also been observed in pure mechanical models (Messina, 2005, 2011; Messina and Rollo, 2010) and is validated now in multiphysics cases.

The agreement between the results of both models is clearly shown in Tables 3 and 4. However, when the comparison is extended to the results given by Heyliger and Saravanos (1995) (second column in Tables 3 and 4), a slightly lower quality can be noticed in the comparisons. Perusal of Tables 3 and 4 has in fact revealed several Heyliger and Saravanos (1995) values that are in slight disagreement with those achieved herein. In total, 50% of the values provided by Heyliger and Saravanos (1995) agree for about only 3–4 significant digits. Such a disagreement could of course be considered slight, within the frame of engineering interest.

Table 2. Geometrical properties of single- and multi-layered plates (h = 10 mm).

Ref.	Material (ref. Table 1)	Material orientation (°)	Thicknesses (mm)
Pa	m_2	0	10
Pb	$m_2/m_3/m_3/m_3/m_2$	0/0/90/0/0	$1/\frac{8}{3}/\frac{8}{3}/\frac{8}{3}/1$
Pc	$m_1/m_2/m_2/m_1$	0/0/0/0	$\frac{5}{2}/\frac{5}{2}/\frac{5}{2}/\frac{5}{2}$
Pd	$m_2/m_1/m_1/m_2$	0/0/0/0	$\frac{5}{2}/\frac{5}{2}/\frac{5}{2}/\frac{5}{2}$

Table 3. First eigenvalues (ω/100) for square Pa-plate with $m = n = 1$ and $\varphi = 0$ at bottom and top of the plate.

L_x/h = 1	Heyliger and Saravanos (1995)	Exact analysis, W_φ			Virtual displacements and GPSFs, $N_o(N)$ for N_L = 2			Virtual displacements, N		
		10^6	10^9	10^{12}	4(7)	6(11)	8(15)	6	8	10
1	713,061	713,023	713,023	713,023	713,475	713,023	713,023	713,072	713,023	713,023
2	777,021	777,021	777,021	777,021	777,446	777,021	777,021	777,021	777,021	777,021
3	889,902	889,882	889,882	889,882	890,015	889,882	889,882	889,883	889,882	889,882
4	925,431	925,431	925,431	925,431	925,783	925,432	925,431	925,432	925,431	925,431
5	1,243,819	1,243,809	1,243,808	1,243,808	1,245,461	1,243,809	1,243,808	1,245,400	1,243,813	1,243,808
6	1,270,594	1,270,594	1,270,594	1,270,594	1,271,040	1,270,594	1,270,594	1,273,476	1,270,607	1,270,594

GPSFs: global piecewise-smooth functions.

Table 4. First eigenvalues (ω/100) for square Pa-plate with $m = n = 1$ and $q = 0$ at bottom and top of the plate.

L_x/h = 1	Heyliger and Saravanos (1995)	Exact analysis, W_φ			Virtual displacements and GPSFs, $N_o(N)$ for N_L = 2			Virtual displacements, N		
		10^6	10^9	10^{12}	4(7)	6(11)	8(15)	6	8	10
1	724,602	724,558	724,558	724,558	725,083	724,558	724,558	724,613	724,558	724,558
2	777,021	777,021	777,021	777,021	777,453	777,021	777,021	777,021	777,021	777,021
3	912,912	912,883	912,883	912,883	913,014	912,883	912,883	912,884	912,883	912,883
4	925,431	925,431	925,431	925,431	925,792	925,432	925,431	925,432	925,431	925,431
5	1,270,594	1,270,594	1,270,594	1,270,594	1,271,043	1,270,594	1,270,594	1,273,476	1,270,607	1,270,594
6	1,293,504	1,293,476	1,293,476	1,293,476	1,296,321	1,293,479	1,293,476	1,296,582	1,293,490	1,293,476

GPSFs: global piecewise-smooth functions.

Table 5. First eigenvalues (ω/100) for square Pa-plate with $m = n = 1$ and $\varphi = 0$ at bottom and top of the plate.

	Heyliger and Saravanos (1995)	Exact analysis, W_φ			Virtual displacements, N		
		10^6	10^9	10^{12}	6	8	10
$L_x/h = 4$							
1	96,929.9	96,926.7	96,926.7	96,926.7	96,926.7	96,926.7	96,926.7
2	194,255	194,255	194,255	194,255	194,255	194,255	194,255
3	327,663	327,663	327,663	327,663	327,663	327,663	327,663
4	538,885	538,885	538,885	538,885	538,885	538,885	538,885
5	609,186	609,186	609,186	609,186	609,190	609,186	609,186
6	958,922	958,919	958,919	958,919	960,384	958,923	958,919
$L_x/h = 10$							
1	18,013.4	18,012.9	18,012.9	18,012.9	18,012.9	18,012.9	18,012.9
2	77,702.1	77,702.1	77,702.1	77,702.1	77,702.1	77,702.1	77,702.1
3	133,695	133,695	133,695	133,695	133,695	133,695	133,695
4	508,625	508,625	508,625	508,625	508,625	508,625	508,625
5	522,320	522,320	522,320	522,320	522,320	522,320	522,320
6	988,021	988,020	988,020	988,020	990,583	988,030	988,020
$L_x/h = 50$							
1	746.752	746.731	746.731	746.731	746.731	746.731	746.731
2	15,540.4	15,540.4	15,540.4	15,540.4	15,540.4	15,540.4	15,540.4
3	26,828.0	26,828.0	26,828.0	26,828.0	26,828.0	26,828.0	26,828.0
4	502,895	502,895	502,895	502,895	502,895	502,895	502,895
5	503,469	503,469	503,469	503,469	503,469	503,469	503,469
6	1,004,344	1,004,344	1,004,344	1,004,344	1,004,990	1,004,360	1,004,344

Table 6. First eigenvalues (ω/100) for square Pa-plate with $m = n = 1$ and $q = 0$ at bottom and top of the plate.

	Heyliger and Saravanos (1995)	Exact analysis, W_φ			Virtual displacements, N		
		10^6	10^9	10^{12}	6	8	10
$L_x/h = 4$							
1	98,231.7	98,227.9	98,228.0	98,228.0	98,228.0	98,228.0	98,228.0
2	194,255	194,255	194,255	194,255	194,255	194,255	194,255
3	355,110	355,100	355,100	355,100	355,100	355,100	355,100
4	538,885	538,885	538,885	538,885	538,885	538,885	538,885
5	690,767	690,735	690,735	690,735	690,750	690,735	690,735
6	960,103	960,100	960,099	960,099	961,638	960,105	960,099
$L_x/h = 10$							
1	18,077.8	18,077.2	18,077.2	18,077.2	18,077.2	18,077.2	18,077.2
2	77,702.1	77,702.1	77,702.1	77,702.1	77,702.1	77,702.1	77,702.1
3	145,221	145,217	145,217	145,217	145,217	145,217	145,217
4	508,625	508,625	508,625	508,625	508,625	508,625	508,625
5	604,752	604,718	604,718	604,718	604,720	604,718	604,718
6	990,953	990,951	990,951	990,951	993,778	990,963	990,951
$L_x/h = 50$							
1	746.873	746.851	746.851	746.851	746.851	746.851	746.851
2	15,540.4	15,540.4	15,540.4	15,540.4	15,540.4	15,540.4	15,540.4
3	29,153.3	29,152.5	29,152.5	29,152.5	29,152.5	29,152.5	29,152.5
4	502,895	502,895	502,895	502,895	502,895	502,895	502,895
5	586,240	586,207	586,207	586,207	586,207	586,207	586,207
6	1,004,612	1,004,612	1,004,612	1,004,612	1,004,705	1,004,629	1,004,612

However, the case becomes of greater interest when approximate analytical/numerical models need validation with highly accurate exact results.

The excellent agreement between the here-presented models would seem to suggest that the present exact results are more accurate than those previously published.

Tables 5 and 6 extend the simulations presented in Tables 3 and 4 to different length-to-thickness ratios. The same weights (10^6, 10^9, 10^{12}) have been used in

Table 7. First eigenvalues (ω/100) for square Pc and Pd plates with $m = n = 1$ and $\varphi = 0$ at bottom and top of the plate.

	Heyliger and Saravanos (1995)	Exact analysis $W_\varphi = 10^9$	GPSFs $N_o = 6$ ($N = 21$)
$L_x/h = 4$; Pc-plate			
1	72,174.4	72,173.2	72,173.2
2	194,760	194,759	194,759
3	306,209	306,208	306,208
4	337,107	337,104	337,104
5	424,602	424,598	424,598
6	529,129	529,127	529,127
$L_x/h = 50$; Pc-plate			
1	633.417	633.414	633.414
2	16,431.1	16,431.0	16,431.0
3	28,535.2	28,534.9	28,534.9
4	268,118	268,118	268,118
5	353,079	353,079	353,079
6	369,396	369,396	369,396
$L_x/h = 4$; Pd-plate			
1	58,248.7	58,248.1	58,248.1
2	192,408	192,406	192,406
3	271,757	271,756	271,756
4	329,584	329,582	329,582
5	363,048	363,047	363,047
6	406,665	406,660	406,660
$L_x/h = 50$; Pd-plate			
1	725.219	725.201	725.201
2	16,430.2	16,430.0	16,430.0
3	28,535.7	28,535.4	28,535.4
4	159,732	159,731	159,731
5	226,218	226,218	226,218
6	353,386	353,386	353,386

GPSFs: global piecewise-smooth functions.

Table 8. First eigenvalues (ω/100) for square Pc and Pd plates with $m = n = 1$ and $q = 0$ at bottom and top of the plate.

	Heyliger and Saravanos (1995)	Exact analysis, $W_\varphi = 10^9$	GPSFs, $N_o = 6$ ($N = 21$)
$L_x/h = 4$; Pc-plate			
1	72,191.5	72,190.3	72,190.3
2	194,881	194,880	194,880
3	306,539	306,538	306,538
4	337,196	337,193	337,193
5	424,664	424,660	424,660
6	529,543	529,541	529,541
$L_x/h = 50$; Pc-plate			
1	633.487	633.484	633.484
2	16,440.9	16,440.7	16,440.7
3	28,555.3	28,555.0	28,555.0
4	271,222	271,221	271,221
5	362,248	362,244	362,244
6	369,397	369,396	369,396
$L_x/h = 4$; Pd-plate			
1	58,354.0	58,353.3	58,353.3
2	192,346	192,435	192,435
3	271,758	271,756	271,756
4	329,593	329,591	329,591
5	364,072	364,071	364,071
6	407,771	407,765	407,765.50
$L_x/h = 50$; Pd-plate			
1	725.241	725.223	725.223
2	16,438.8	16,438.7	16,438.7
3	28,555.1	28,554.7	28,554.7
4	159,865	159,865	159,865
5	226,643	226,643	226,643
6	363,810	363,803	363,803

GPSFs: global piecewise-smooth functions.

these tables to extract exact results, while the approximate 3D analysis uses classical orthogonal polynomials expanded intra the single homogeneous layer of the Pa-plate. Tables 5 and 6 clearly show an excellent stability and agreement between both the exact and approximate results. The ability of the exact approach to identically extract the first six significant digits, regardless of which weight is used, is worth mentioning. Finally, the excellent behaviour of both models, irrespective of the length-to-thickness ratio, is clearly illustrated in both Tables 5 and 6. However, when the results extracted by the present models are compared with those achieved by Heyliger and Saravanos (1995), differences can be observed. In particular, these differences are more pronounced when a nil electric charge is established as the boundary condition at the top and bottom of the plate (Table 6). On average, the first four significant digits agree.

The agreement or disagreement of the comparisons carried out with respect to Heyliger and Saravanos (1995) essentially seem to be influenced by the relationship between the potential and the displacements. A more detailed examination of Tables 3 to 6, compared to Table 2 (Heyliger and Saravanos, 1995), has in fact revealed a concentration of differences for those eigenvalues whose modes present a higher scaling factor (i.e. the magnitude of the potential to a displacement component ratio), thus revealing the delicateness of the multiphysics problem in the presence of significant electric–mechanical coupling. Such a scaling factor was introduced by Heyliger and Saravanos (1995) to denote the relationship between the potential and the displacement and was termed the specific potential-to-displacement component ratio. Let us now observe Table 3; the eigenvalues 713,061, 889,902 and 1,243,819 in this table are different from those evaluated with the present analysis; the absolute scaling factors published by Heyliger and Saravanos (1995) for these eigenvalues were (1.744×10^9, 1.515×10^{11}, 1.534×10^9), respectively. Conversely, again based on Table 3, no difference exists between the eigenvalues of the present analysis and those of Heyliger and Saravanos (1995) when the compared eigenvalues are associated with nil scaling factors; similar observations can be extended to all the relevant eigenvalues listed in Tables 3 to 6 when compared to those in Table 2 of Heyliger and Saravanos (1995).

On the basis of the stability of the exact method tested in Tables 3 to 6, the subsequent evaluations will use a weight factor $W_\varphi = 10^9$.

Table 9. First eigenvalues (ω/100) for square Pb-plate with $m = n = 1$ and $\varphi = 0$ at bottom and top of the plate.

	Heyliger and Saravanos (1995)	Carrera et al. (2010) (LD4)	Exact analysis, $W_\varphi = 10^9$	GPSFs, $N_o(N)$ for $N_L = 5$		
				4(16)	5(21)	6(26)
$L_x/h = 4$						
1	57,074.5	57,074.0	57,074.0	57,078.4	57,077.9	57,074.0
2	191,301	191,301	191,301	191,361	191,359	191,301
3	250,769	250,768	250,768	250,816	250,813	250,768
4	274,941		274,940	274,982	274,977	274,940
5	362,492		362,489	362,540	362,531	362,489
6	381,036		381,036	381,045	381,042	381,036
$L_x/h = 50$						
1	618.118	618.106	618.105	618.233	618.228	618.105
2	15,681.6	15,681.6	15,681.5	15,686.6	15,686.5	15,681.6
3	21,492.8	21,492.6	21,492.6	21,497.1	21,496.8	21,492.6
4	209,704		209,704	209,705	209,705	209,704
5	210,522		210,522	210,523	210,522	210,522
6	378,104		378,104	378,105	378,104	378,104

GPSFs: global piecewise-smooth functions.

Table 10. First eigenvalues (ω/100) for square Pb-plate with $m = n = 1$ and $q = 0$ at bottom and top of the plate.

	Heyliger and Saravanos (1995)	Exact model, $W_\varphi = 10^9$	GPSFs, $N_o(N)$ for $N_L = 5$		
			4(16)	5(21)	6(26)
$L_x/h = 4$					
1	57,089.3	57,088.7	57,093.2	57,092.7	57,088.7
2	191,304	191,304	191,364	191,362	191,304
3	250,770	250,768	250,817	250,814	250,768
4	274,941	274,940	274,982	274,978	274,940
5	362,522	362,520	362,571	362,561	362,520
6	381,049	381,048	381,057	381,055	381,048
$L_x/h = 50$					
1	618.120	618.108	618.236	618.230	618.108
2	15,681	15,682	15,687	15,687	15,682
3	21,493.0	21,492.8	21,497.3	21,497.0	21,492.8
4	209,707	209,707	209,708	209,708	209,707
5	210,573	210,573	210,573	210,573	210,573
6	378,105	378,105	378,106	378,105	378,105

GPSFs: global piecewise-smooth functions.

In a further attempt to converge to the results derived from the exact procedure illustrated in Heyliger and Saravanos (1995), Tables 7 and 8 analyse a multilayered plate made up of four layers symmetrically placed through the thickness of the plate (i.e. Pc and Pd-plate). These tables still show the presence of a difference from Heyliger and Saravanos (1995), even though it seems to be slightly less than that in Tables 3 to 6. The results achieved with the present exact approach are again coincident with those obtained with the approximate analysis based on GPSFs (Messina, 2002; Messina and Rollo, 2010) through which the displacement components in the thickness direction of the plate are modelled as if the plate were made up of a single layer. This case has again shown that both the exact and the approximate results are mutually validated.

Finally, Tables 9 and 10 could be interesting; these tables consider the eigenvalues associated with a multilayered plate made up of five layers placed symmetrically through the thickness of the plate (i.e. Pb-plate) and which still show perfect coincidence between the converged and exact results up to the first six significant digits. Moreover, the results obtained with the approximate theory developed by Carrera et al. (2010) (i.e. the so-called LD4) compared with both the present values and those obtained by Heyliger and Saravanos (1995) are worth mentioning. The Carrera et al. (2010) values in fact agree more closely with present results than with those of Heyliger and Saravanos (1995).

Finally, the convergence velocity of the present approximate analysis, compared to LD4, should be mentioned. Carrera et al. (2010) used LD4 to approximate

displacement components and the electric potential, at a layer-to-layer level, up to the fourth polynomial order. The present model instead converges to exact results using the sixth order. For this reason, a lower velocity convergence can be attributed to the present model. The present model is *de facto* slower than LD4, because this latter is partially exact. In fact, LD4 only used polynomial approximations through the z-coordinates along with circular (exact) functions through in-plane displacement and potential components. This choice was made because LD4 is only capable of concentrating the analysis on simply supported plates, while the present model has been developed for any classical boundary condition.

Conclusion

Two models that have the aim of analysing 3D freely vibrating piezoelectric/composite multi-layered plates have been introduced and tested in this article.

The first model provides the possibility of investigating (*i*) an arbitrary combination of structural (angle- or cross-ply) and/or piezoelectric layers and (*ii*) plates subjected to any classical boundary condition and (*iii*) allows 3D-results to be obtained for any degree of accuracy. This first model is (*iv*) able to model the plates as if they were virtually made up of a single layer. The theoretical basis of the model consists in using GPSFs (for both mechanical and electric quantities), along with the classical theorem of virtual displacements.

The second model is an exact method which has been developed within the frame of electric/mechanical simply supported boundary conditions. The model has been described along with its ability to overcome numerical instabilities, which can be due to the different physical quantities involved in the multiphysics problem. As the method is immediately implementable in modern computers, it could be used effectively to assist investigations and provide reliable exact results, where needed.

Numerical simulations have provided exact results that have been mutually validated and compared with previous results. The accuracy of the new results has been proved, and the results have been presented for the benchmarking of comparisons.

Acknowledgements

Heyliger and Saravanos (1995) are gratefully acknowledged for having pioneered and provided an extended numerical data set. This numerical set has allowed the authors of this article to single out the numerical instabilities that can characterize the multiphysics problem which has been dealt with.

Declaration of conflicting interests

The authors declared no potential conflicts of interest with respect to the research, authorship, and/or publication of this article.

Funding

This research received no specific grant from any funding agency in the public, commercial or not-for-profit sectors.

References

Ballhause D, D'Ottavio M, Kröplin B, et al. (2005) A unified formulation to assess multilayered theories for piezoelectric plates. *Computers & Structures* 83: 1217–1235.

Batra RC and Liang XQ (1997) The vibration of a rectangular laminated elastic plate with embedded piezoelectric sensors and actuators. *Computers & Structures* 63(2): 203–2016.

Boyce WE and DiPrima C (1997) *Elementary Differential Equations and Boundary Value Problems*. New York: John Wiley & Sons.

Carrera E, Brischetto S and Cinefra M (2010) Variable kinematics and variational statements for free vibrations analysis of piezoelectric plates and shells. *Computer Modeling in Engineering & Sciences* 65(3): 259–341.

Chen W-Q, Xu R-Q and Ding H-J (1998) On free vibration of a piezoelectric composite rectangular plate. *Journal of Sound and Vibration* 218(4): 741–748.

Cupial P (2005) Three-dimensional natural vibration analysis and energy considerations for a piezoelectric rectangular plate. *Journal of Sound and Vibration* 283: 1093–1113.

Deü J-F and Benjeddou A (2005) Free-vibration analysis of laminated plates with embedded shear-mode piezoceramic layers. *International Journal of Solids and Structures* 42: 2059–2088.

D'Ottavio M and Kröplin B (2006) An extension of Reissner mixed variational theorem to piezoelectric laminates. *Mechanics of Advanced Materials and Structures* 13: 139–150.

Fan J and Ye JQ (1990) An exact solution for the static and dynamics of laminated thick plates with orthotropic layers. *International Journal of Solids and Structures* 26: 655–662.

Heyliger P and Saravanos DA (1995) Exact free-vibration analysis of laminated plates with embedded piezoelectric plates. *Journal of the Acoustical Society of America* 98(3): 1547–1557.

Liang XQ and Batra RC (1997) Changes in frequencies of a laminated plate caused by embedded piezoelectric layers. *AIAA Journal* 35(10): 1672–1673.

Messina A (2002) Free vibrations of multilayered plates on the base of a mixed variational approach in conjunction with global piecewise-smooth functions. *Journal of Sound and Vibration* 256(1): 103–129.

Messina A (2005) Free vibrations analysis of multilayered plates; mixed against displacement-based formulations. In: *EURODYN 2005 – VI European conference on structural dynamics (internal symposia organized by M Petyt)* (ed C Soize and GI Schueller, Millpress, Rotterdam, ISBN: 9059660331), Paris, 4–7 September, pp. 1141–1147.

Messina A (2011) Influence of the edge-boundary conditions on three-dimensional free vibrations of isotropic and cross-ply multilayered rectangular plates. *Composite Structures* 93: 2135–2151.

Messina A (2012) Three-dimensional free vibration analysis of cross-ply laminated rectangular plates through 2D and

exact models. *Mechanics of Advanced Materials and Structures* 19: 250–264.
Messina A and Rollo G (2010) Three-dimensional free vibration analysis of cross-ply laminated rectangular plates with free edges through a displacement-based approach. *Mathematics and Mechanics of Solids* 15: 539–556.
Mindlin RD (1952) Forced thickness shear and flexural vibrations of piezoelectric crystal plates. *Journal of Applied Physics* 23: 83–88.
Mindlin RD (1972) High frequency vibrations of piezoelectric crystal plates. *International Journal of Solids and Structures* 8: 895–906.
Reissner E (1984) On a certain mixed variational theory and a proposed application. *International Journal for Numerical Methods in Engineering* 20: 1366–1368.
Vel SS and Batra RC (2000) Three-dimensional analytical solution for hybrid multilayered piezoelectric plates. *Journal of Applied Mechanics: Transactions of the ASME* 67: 558–567.
Vel SS and Batra RC (2001) Exact solutions for rectangular sandwich plates with embedded piezoelectric shear actuators. *AIAA Journal* 39(10): 1363–1373.
Yang JS and Batra RC (1994) Free vibrations of a piezoelectric body. *Journal of Elasticity* 34: 239–254.

Appendix I

The eigenvalue problem in section 'The approximate analysis' is obtained as follows

$$\left[\begin{bmatrix} \mathbf{K}^{uu} & \mathbf{K}^{uv} & \mathbf{K}^{uw} & \mathbf{K}^{u\phi} \\ & \mathbf{K}^{vv} & \mathbf{K}^{vw} & \mathbf{K}^{v\varphi} \\ & & \mathbf{K}^{ww} & \mathbf{K}^{w\varphi} \\ sym & & & \mathbf{K}^{\varphi\varphi} \end{bmatrix} - \omega^2 \cdot \begin{bmatrix} \mathbf{M}^{u} & \mathbf{0} & \mathbf{0} & \mathbf{0} \\ & \mathbf{M}^{v} & \mathbf{0} & \mathbf{0} \\ & & \mathbf{M}^{w} & \mathbf{0} \\ sym & & & \mathbf{0} \end{bmatrix}\right] \cdot \begin{pmatrix} \mathbf{A}^{u} \\ \mathbf{A}^{v} \\ \mathbf{A}^{w} \\ \mathbf{A}^{\varphi} \end{pmatrix} = (\mathbf{0}) \tag{31}$$

or in its reduced form. The reduced form can be achieved by taking into account the fourth row in (31)

$$\mathbf{K}^{u\varphi^{\mathrm{T}}} \cdot \mathbf{A}^{u} + \mathbf{K}^{v\varphi^{\mathrm{T}}} \cdot \mathbf{A}^{v} + \mathbf{K}^{w\varphi^{\mathrm{T}}} \cdot \mathbf{A}^{w} + \mathbf{K}^{\varphi\varphi} \cdot \mathbf{A}^{\varphi} = (\mathbf{0}) \tag{32}$$

from which the vector $(\mathbf{A}^{\varphi})$ can be written as depending on $\mathbf{A}^{u}$, $\mathbf{A}^{v}$ and $\mathbf{A}^{w}$

$$\mathbf{A}^{\varphi} = -\mathbf{K}^{\varphi\varphi^{-1}} \cdot \mathbf{K}^{u\varphi^{\mathrm{T}}} \cdot \mathbf{A}^{u} - \mathbf{K}^{\varphi\varphi^{-1}} \cdot \mathbf{K}^{v\varphi^{\mathrm{T}}} \cdot \mathbf{A}^{v} - \mathbf{K}^{\varphi\varphi^{-1}} \cdot \mathbf{K}^{w\varphi^{\mathrm{T}}} \cdot \mathbf{A}^{w} \tag{33}$$

Once equation (33) is in turn substituted in the first three rows of (31), a reduced eigenvalue problem is achieved as in equation (34)

$$\left[\begin{bmatrix} \mathbf{K}^{uu} - \mathbf{K}^{u\varphi} \cdot \mathbf{K}^{\varphi\varphi^{-1}} \cdot \mathbf{K}^{u\varphi^{\mathrm{T}}} & \mathbf{K}^{uv} - \mathbf{K}^{u\varphi} \cdot \mathbf{K}^{\varphi\varphi^{-1}} \cdot \mathbf{K}^{v\varphi^{\mathrm{T}}} & \mathbf{K}^{uw} - \mathbf{K}^{u\varphi} \cdot \mathbf{K}^{\varphi\varphi^{-1}} \cdot \mathbf{K}^{w\varphi^{\mathrm{T}}} \\ & \mathbf{K}^{vv} - \mathbf{K}^{v\varphi} \cdot \mathbf{K}^{\varphi\varphi^{-1}} \cdot \mathbf{K}^{v\varphi^{\mathrm{T}}} & \mathbf{K}^{vw} - \mathbf{K}^{v\varphi} \cdot \mathbf{K}^{\varphi\varphi^{-1}} \cdot \mathbf{K}^{w\varphi^{\mathrm{T}}} \\ sym & & \mathbf{K}^{ww} - \mathbf{K}^{w\varphi} \cdot \mathbf{K}^{\varphi\varphi^{-1}} \cdot \mathbf{K}^{w\varphi^{\mathrm{T}}} \end{bmatrix} - \omega^2 \cdot \begin{bmatrix} \mathbf{M}^{u} & \mathbf{0} & \mathbf{0} \\ & \mathbf{M}^{v} & \mathbf{0} \\ sym & & \mathbf{M}^{w} \end{bmatrix}\right] \cdot \begin{pmatrix} \mathbf{A}^{u} \\ \mathbf{A}^{v} \\ \mathbf{A}^{w} \end{pmatrix} = (\mathbf{0}) \tag{34}$$

The sub-matrices can be obtained by carrying out the following integrations

$$\mathbf{M}^{\alpha} = \int_{Vol} \rho(\mathbf{X}^{\alpha}\mathbf{Y}^{\alpha}\mathbf{Z}^{\alpha}) \cdot (\mathbf{X}^{\alpha}\mathbf{Y}^{\alpha}\mathbf{Z}^{\alpha})^{\mathrm{T}} \mathrm{d}Vol \quad \text{with } \alpha = u, v, w$$

$$\begin{aligned} \mathbf{K}^{uu} = \int_{Vol} & C_{11}(\mathbf{X}^{u\prime}\mathbf{Y}^{u}\mathbf{Z}^{u}) \cdot (\mathbf{X}^{u\prime}\mathbf{Y}^{u}\mathbf{Z}^{u})^{\mathrm{T}} + C_{16}(\mathbf{X}^{u\prime}\mathbf{Y}^{u}\mathbf{Z}^{u}) \cdot (\mathbf{X}^{u}\mathbf{Y}^{u\prime}\mathbf{Z}^{u})^{\mathrm{T}} + \\ & + C_{16}(\mathbf{X}^{u}\mathbf{Y}^{u\prime}\mathbf{Z}^{u}) \cdot (\mathbf{X}^{u\prime}\mathbf{Y}^{u}\mathbf{Z}^{u})^{\mathrm{T}} + C_{66}(\mathbf{X}^{u}\mathbf{Y}^{u\prime}\mathbf{Z}^{u}) \cdot (\mathbf{X}^{u}\mathbf{Y}^{u\prime}\mathbf{Z}^{u})^{\mathrm{T}} + \\ & + C_{55}(\mathbf{X}^{u}\mathbf{Y}^{u}\mathbf{Z}^{u\prime}) \cdot (\mathbf{X}^{u}\mathbf{Y}^{u}\mathbf{Z}^{u\prime})^{\mathrm{T}} \mathrm{d}Vol \end{aligned}$$

$$
\begin{aligned}
\mathbf{K}^{uv} = & \int_{Vol} C_{12}(\mathbf{X}^{u\prime}\mathbf{Y}^{u}\mathbf{Z}^{u})\cdot(\mathbf{X}^{v}\mathbf{Y}^{v\prime}\mathbf{Z}^{v})^{\mathrm{T}} + C_{16}(\mathbf{X}^{u\prime}\mathbf{Y}^{u}\mathbf{Z}^{u})\cdot(\mathbf{X}^{v\prime}\mathbf{Y}^{v}\mathbf{Z}^{v})^{\mathrm{T}} + \\
& + C_{26}(\mathbf{X}^{u}\mathbf{Y}^{u\prime}\mathbf{Z}^{u})\cdot(\mathbf{X}^{v}\mathbf{Y}^{v\prime}\mathbf{Z}^{v})^{\mathrm{T}} + C_{66}(\mathbf{X}^{u}\mathbf{Y}^{u\prime}\mathbf{Z}^{u})\cdot(\mathbf{X}^{v\prime}\mathbf{Y}^{v}\mathbf{Z}^{v})^{\mathrm{T}} + \\
& + C_{45}(\mathbf{X}^{u}\mathbf{Y}^{u}\mathbf{Z}^{u\prime})\cdot(\mathbf{X}^{v}\mathbf{Y}^{v}\mathbf{Z}^{v\prime})^{\mathrm{T}}\mathrm{d}Vol \\
\mathbf{K}^{uw} = & \int_{Vol} C_{13}(\mathbf{X}^{u\prime}\mathbf{Y}^{u}\mathbf{Z}^{u})\cdot(\mathbf{X}^{w}\mathbf{Y}^{w}\mathbf{Z}^{w\prime})^{\mathrm{T}} + C_{36}(\mathbf{X}^{u}\mathbf{Y}^{u\prime}\mathbf{Z}^{u})\cdot(\mathbf{X}^{w}\mathbf{Y}^{w}\mathbf{Z}^{w\prime})^{\mathrm{T}} + \\
& + C_{45}(\mathbf{X}^{u}\mathbf{Y}^{u}\mathbf{Z}^{u\prime})\cdot(\mathbf{X}^{w}\mathbf{Y}^{w\prime}\mathbf{Z}^{w})^{\mathrm{T}} + C_{55}(\mathbf{X}^{u}\mathbf{Y}^{u}\mathbf{Z}^{u\prime})\cdot(\mathbf{X}^{w\prime}\mathbf{Y}^{w}\mathbf{Z}^{w})^{\mathrm{T}}\mathrm{d}Vol \\
\mathbf{K}^{u\varphi} = & \int_{Vol} e_{31}(\mathbf{X}^{u\prime}\mathbf{Y}^{u}\mathbf{Z}^{u})\cdot(\mathbf{X}^{\varphi}\mathbf{Y}^{\varphi}\mathbf{Z}^{\varphi\prime})^{\mathrm{T}} + e_{36}(\mathbf{X}^{u}\mathbf{Y}^{u\prime}\mathbf{Z}^{u})\cdot(\mathbf{X}^{\varphi}\mathbf{Y}^{\varphi}\mathbf{Z}^{\varphi\prime})^{\mathrm{T}} + \\
& + e_{15}(\mathbf{X}^{u}\mathbf{Y}^{u}\mathbf{Z}^{u\prime})\cdot(\mathbf{X}^{\varphi\prime}\mathbf{Y}^{\varphi}\mathbf{Z}^{\varphi})^{\mathrm{T}} + e_{25}(\mathbf{X}^{u}\mathbf{Y}^{u}\mathbf{Z}^{u\prime})\cdot(\mathbf{X}^{\varphi}\mathbf{Y}^{\varphi\prime}\mathbf{Z}^{\varphi})^{\mathrm{T}}\mathrm{d}Vol \\
\mathbf{K}^{vv} = & \int_{Vol} C_{26}(\mathbf{X}^{v\prime}\mathbf{Y}^{v}\mathbf{Z}^{v})\cdot(\mathbf{X}^{v}\mathbf{Y}^{v\prime}\mathbf{Z}^{v})^{\mathrm{T}} + C_{66}(\mathbf{X}^{v\prime}\mathbf{Y}^{v}\mathbf{Z}^{v})\cdot(\mathbf{X}^{v\prime}\mathbf{Y}^{v}\mathbf{Z}^{v})^{\mathrm{T}} + \\
& + C_{22}(\mathbf{X}^{v}\mathbf{Y}^{v\prime}\mathbf{Z}^{v})\cdot(\mathbf{X}^{v}\mathbf{Y}^{v\prime}\mathbf{Z}^{v})^{\mathrm{T}} + C_{26}(\mathbf{X}^{v}\mathbf{Y}^{v\prime}\mathbf{Z}^{v})\cdot(\mathbf{X}^{v\prime}\mathbf{Y}^{v}\mathbf{Z}^{v})^{\mathrm{T}} + \\
& + C_{44}(\mathbf{X}^{v}\mathbf{Y}^{v}\mathbf{Z}^{v\prime})\cdot(\mathbf{X}^{v}\mathbf{Y}^{v}\mathbf{Z}^{v\prime})^{\mathrm{T}}\mathrm{d}Vol \\
\mathbf{K}^{vw} = & \int_{Vol} C_{36}(\mathbf{X}^{v\prime}\mathbf{Y}^{v}\mathbf{Z}^{v})\cdot(\mathbf{X}^{w}\mathbf{Y}^{w}\mathbf{Z}^{w\prime})^{\mathrm{T}} + C_{23}(\mathbf{X}^{v}\mathbf{Y}^{v\prime}\mathbf{Z}^{v})\cdot(\mathbf{X}^{w}\mathbf{Y}^{w}\mathbf{Z}^{w\prime})^{\mathrm{T}} + \\
& + C_{45}(\mathbf{X}^{v}\mathbf{Y}^{v}\mathbf{Z}^{v\prime})\cdot(\mathbf{X}^{w\prime}\mathbf{Y}^{w}\mathbf{Z}^{w})^{\mathrm{T}} + C_{44}(\mathbf{X}^{v}\mathbf{Y}^{v}\mathbf{Z}^{v\prime})\cdot(\mathbf{X}^{w}\mathbf{Y}^{w\prime}\mathbf{Z}^{w})^{\mathrm{T}}\mathrm{d}Vol \\
\mathbf{K}^{v\varphi} = & \int_{Vol} e_{36}(\mathbf{X}^{v\prime}\mathbf{Y}^{v}\mathbf{Z}^{v})\cdot(\mathbf{X}^{\varphi}\mathbf{Y}^{\varphi}\mathbf{Z}^{\varphi\prime})^{\mathrm{T}} + e_{32}(\mathbf{X}^{v}\mathbf{Y}^{v\prime}\mathbf{Z}^{v})\cdot(\mathbf{X}^{\varphi}\mathbf{Y}^{\varphi}\mathbf{Z}^{\varphi\prime})^{\mathrm{T}} + \\
& + e_{14}(\mathbf{X}^{v}\mathbf{Y}^{v}\mathbf{Z}^{v\prime})\cdot(\mathbf{X}^{\varphi\prime}\mathbf{Y}^{\varphi}\mathbf{Z}^{\varphi})^{\mathrm{T}} + e_{24}(\mathbf{X}^{v}\mathbf{Y}^{v}\mathbf{Z}^{v\prime})\cdot(\mathbf{X}^{\varphi}\mathbf{Y}^{\varphi\prime}\mathbf{Z}^{\varphi})^{\mathrm{T}}\mathrm{d}Vol \\
\mathbf{K}^{ww} = & \int_{Vol} C_{45}(\mathbf{X}^{w\prime}\mathbf{Y}^{w}\mathbf{Z}^{w})\cdot(\mathbf{X}^{w}\mathbf{Y}^{w\prime}\mathbf{Z}^{w})^{\mathrm{T}} + C_{55}(\mathbf{X}^{w\prime}\mathbf{Y}^{w}\mathbf{Z}^{w})\cdot(\mathbf{X}^{w\prime}\mathbf{Y}^{w}\mathbf{Z}^{w})^{\mathrm{T}} + \\
& + C_{44}(\mathbf{X}^{w}\mathbf{Y}^{w\prime}\mathbf{Z}^{w})\cdot(\mathbf{X}^{w}\mathbf{Y}^{w\prime}\mathbf{Z}^{w})^{\mathrm{T}} + C_{45}(\mathbf{X}^{w}\mathbf{Y}^{w\prime}\mathbf{Z}^{w})\cdot(\mathbf{X}^{w\prime}\mathbf{Y}^{w}\mathbf{Z}^{w})^{\mathrm{T}} + \\
& + C_{33}(\mathbf{X}^{w}\mathbf{Y}^{w}\mathbf{Z}^{w\prime})\cdot(\mathbf{X}^{w}\mathbf{Y}^{w}\mathbf{Z}^{w\prime})^{\mathrm{T}}\mathrm{d}Vol \\
\mathbf{K}^{w\varphi} = & \int_{Vol} e_{15}(\mathbf{X}^{w\prime}\mathbf{Y}^{w}\mathbf{Z}^{w})\cdot(\mathbf{X}^{\varphi\prime}\mathbf{Y}^{\varphi}\mathbf{Z}^{\varphi})^{\mathrm{T}} + e_{25}(\mathbf{X}^{w\prime}\mathbf{Y}^{w}\mathbf{Z}^{w})\cdot(\mathbf{X}^{\varphi}\mathbf{Y}^{\varphi\prime}\mathbf{Z}^{\varphi})^{\mathrm{T}} + \\
& + e_{14}(\mathbf{X}^{w}\mathbf{Y}^{w\prime}\mathbf{Z}^{w})\cdot(\mathbf{X}^{\varphi\prime}\mathbf{Y}^{\varphi}\mathbf{Z}^{\varphi})^{\mathrm{T}} + e_{24}(\mathbf{X}^{w}\mathbf{Y}^{w\prime}\mathbf{Z}^{w})\cdot(\mathbf{X}^{\varphi}\mathbf{Y}^{\varphi\prime}\mathbf{Z}^{\varphi})^{\mathrm{T}} + \\
& + e_{33}(\mathbf{X}^{w}\mathbf{Y}^{w}\mathbf{Z}^{w\prime})\cdot(\mathbf{X}^{\varphi}\mathbf{Y}^{\varphi}\mathbf{Z}^{\varphi\prime})^{\mathrm{T}}\mathrm{d}Vol \\
\mathbf{K}^{\varphi\varphi} = & -\int_{Vol} \in_{1}(\mathbf{X}^{\varphi\prime}\mathbf{Y}^{\varphi}\mathbf{Z}^{\varphi})\cdot(\mathbf{X}^{\varphi\prime}\mathbf{Y}^{\varphi}\mathbf{Z}^{\varphi})^{\mathrm{T}} + \in_{2}(\mathbf{X}^{\varphi}\mathbf{Y}^{\varphi\prime}\mathbf{Z}^{\varphi})\cdot(\mathbf{X}^{\varphi}\mathbf{Y}^{\varphi\prime}\mathbf{Z}^{\varphi})^{\mathrm{T}} + \\
& + \in_{3}(\mathbf{X}^{\varphi}\mathbf{Y}^{\varphi}\mathbf{Z}^{\varphi\prime})\cdot(\mathbf{X}^{\varphi}\mathbf{Y}^{\varphi}\mathbf{Z}^{\varphi\prime})^{\mathrm{T}}\mathrm{d}Vol
\end{aligned}
\tag{35}
$$

being the apexes $()'$ indicative of the ordinary differential operator $\mathrm{d}()/\mathrm{d}(x, y, z)$.

Once integrations in (35) are carried out, the eigenvalue problem (31) or (34) can be solved in order to find the squared circular natural frequencies (ω^2) associated with their respective mechanical modes (A^u, A^v, A^w) whose physical description in the space can be obtained by overlapping equations (8).

Appendix 2

The continuity condition at fixed kth interface and regarding section 'The exact analysis' is obtained as follows

$$\mathbf{F}^{(k+1)}(z_k) = \mathbf{T}(z_k)\cdot\mathbf{F}^{(k)}(z_k) \tag{36}$$

with the transfer matrix $\mathbf{T}$, corresponding at z_k interface, having the following expression

$$\mathbf{T}(z_k) = \mathbf{R}^{(k+1)}\cdot\mathbf{Q}^{(k)} \tag{37}$$

where all the elements different from zero in both matrices $\mathbf{R}^{(k+1)}$ and $\mathbf{Q}^{(k)}$ (referred to the kth layer with $k = 1, \ldots, N_L - 1$) are illustrated in equations (38) to (40). Such a result (equations (36) and (37)) comes directly from imposing the continuity conditions (15) once all the relevant quantities are in advance expressed as a function of displacement components through equations (2), (3), (6) and (16); thus, $\mathbf{R}^{(k+1)}$ corresponds to the inverse of $\mathbf{Q}^{(k+1)}$. However, in this latter regard and in order to avoid any numerical inversion into the model, $\mathbf{R}^{(k+1)}$ has been analytically evaluated and reported in equation (40)

$$
\begin{aligned}
&q^{(k)}_{1,1} = q^{(k)}_{2,2} = q^{(k)}_{3,3} = 1; \;\; q^{(k)}_{4,1} = -q_x C^{(k)}_{13} \\
&q^{(k)}_{4,2} = -q_y C^{(k)}_{23}; \;\; q^{(k)}_{4,7} = C^{(k)}_{33}; \;\; q^{(k)}_{4,8} = e^{(k)}_{33} \\
&q^{(k)}_{5,3} = q_y C^{(k)}_{44}; \;\; q^{(k)}_{5,4} = q_y e^{(k)}_{24}; \;\; q^{(k)}_{5,6} = C^{(k)}_{44} \\
&q^{(k)}_{6,3} = q_x C^{(k)}_{55}; \;\; q^{(k)}_{6,4} = q_x e^{(k)}_{15}; \;\; q^{(k)}_{6,5} = C^{(k)}_{44} \\
&q^{(k)}_{7,4} = 1; \;\; q^{(k)}_{8,1} = -q_x e^{(k)}_{31}; \;\; q^{(k)}_{8,2} = -q_y e^{(k)}_{32}; \;\; q^{(k)}_{8,7} = e^{(k)}_{33} \\
&q^{(k)}_{8,8} = -\in^{(k)}_{3}
\end{aligned}
\tag{38}
$$

$$
\begin{aligned}
&Q^{(k)}_{i,j} = q^{(k)}_{i,j}; \quad \text{for } i,j = 1, \ldots, 8; \; j \neq (4,8) \\
&Q^{(k)}_{i,j} = W_\varphi q^{(k)}_{i,j}; \quad \text{for } i = 1, \ldots, 8; \; j = (4,8)
\end{aligned}
\tag{39}
$$

$$
\begin{aligned}
&R^{(k+1)}_{1,1} = R^{(k+1)}_{2,2} = R^{(k+1)}_{3,3} = 1; \;\; R^{(k+1)}_{4,7} = 1/W_\varphi \\
&R^{(k+1)}_{5,3} = -\frac{q^{(k+1)}_{6,3}}{q^{(k+1)}_{6,5}}; \;\; R^{(k+1)}_{5,6} = \frac{1}{q^{(k+1)}_{6,5}}; \;\; R^{(k+1)}_{5,7} = -\frac{q^{(k+1)}_{6,4}}{q^{(k+1)}_{6,5}} \\
&R^{(k+1)}_{6,3} = -\frac{q^{(k+1)}_{5,3}}{q^{(k+1)}_{5,6}}; \;\; R^{(k+1)}_{6,5} = \frac{1}{q^{(k+1)}_{5,6}}; \;\; R^{(k+1)}_{6,7} = -\frac{q^{(k+1)}_{5,4}}{q^{(k+1)}_{5,6}} \\
&R^{(k+1)}_{7,1} = -\frac{q^{(k+1)}_{4,1} \cdot q^{(k+1)}_{8,8} - q^{(k+1)}_{8,1} \cdot q^{(k+1)}_{4,8}}{q^{(k+1)}_{4,7} \cdot q^{(k+1)}_{8,8} - q^{(k+1)}_{4,8} \cdot q^{(k+1)}_{8,7}}; \;\; R^{(k+1)}_{7,2} = -\frac{q^{(k+1)}_{4,2} \cdot q^{(k+1)}_{8,8} - q^{(k+1)}_{8,2} \cdot q^{(k+1)}_{4,8}}{q^{(k+1)}_{4,7} \cdot q^{(k+1)}_{8,8} - q^{(k+1)}_{4,8} \cdot q^{(k+1)}_{8,7}} \\
&R^{(k+1)}_{7,4} = \frac{q^{(k+1)}_{8,8}}{q^{(k+1)}_{4,7} \cdot q^{(k+1)}_{8,8} - q^{(k+1)}_{4,8} \cdot q^{(k+1)}_{8,7}}; \;\; R^{(k+1)}_{7,8} = -\frac{q^{(k+1)}_{4,8}}{q^{(k+1)}_{4,7} \cdot q^{(k+1)}_{8,8} - q^{(k+1)}_{4,8} \cdot q^{(k+1)}_{8,7}} \\
&R^{(k+1)}_{8,1} = \frac{q^{(k+1)}_{4,1} \cdot q^{(k+1)}_{8,7} - q^{(k+1)}_{8,1} \cdot q^{(k+1)}_{4,7}}{W_\varphi \cdot (q^{(k+1)}_{4,7} \cdot q^{(k+1)}_{8,8} - q^{(k+1)}_{4,8} \cdot q^{(k+1)}_{8,7})}; \;\; R^{(k+1)}_{8,2} = \frac{q^{(k+1)}_{4,2} \cdot q^{(k+1)}_{8,7} - q^{(k+1)}_{8,2} \cdot q^{(k+1)}_{4,7}}{W_\varphi \cdot (q^{(k+1)}_{4,7} \cdot q^{(k+1)}_{8,8} - q^{(k+1)}_{4,8} \cdot q^{(k+1)}_{8,7})} \\
&R^{(k+1)}_{8,4} = -\frac{q^{(k+1)}_{8,7}}{W_\varphi \cdot (q^{(k+1)}_{4,7} \cdot q^{(k+1)}_{8,8} - q^{(k+1)}_{4,8} \cdot q^{(k+1)}_{8,7})}; \;\; R^{(k+1)}_{8,8} = \frac{q^{(k+1)}_{4,7}}{W_\varphi \cdot (q^{(k+1)}_{4,7} \cdot q^{(k+1)}_{8,8} - q^{(k+1)}_{4,8} \cdot q^{(k+1)}_{8,7})}
\end{aligned}
\tag{40}
$$